Functionally Graded Multilayer Composites Based on Poly(D,L lactide)/Bioactive Fillers Fabricated by a 3D Direct Pellet Printing Multi-Extrusion Process

Xavier Lacambra Andreu, Jean-Marc Chenal, Abderrahim Maazou, Khalid Lamnawar

Functionally Graded Multilayer Composites Based on Poly(D,L lactide)/Bioactive Fillers Fabricated by a 3D Direct Pellet Printing Multi-Extrusion Process

Xavier Lacambra Andreu, Jean-Marc Chenal, Abderrahim Maazou, Khalid Lamnawar

ACS Applied Polymer Materials
Msc: ap2c01475

The following graphic will be used for the TOC:

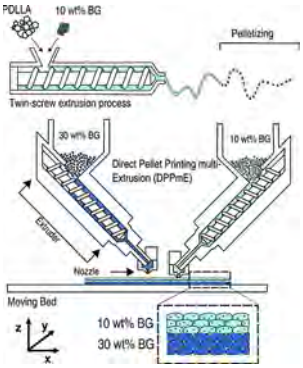

Functionally Graded Multilayer Composites Based on Poly(D,L lactide)/Bioactive Fillers Fabricated by a 3D Direct Pellet Printing Multi-Extrusion Process

Xavier Lacambra Andreu, Jean-Marc Chenal,* Abderrahim Maazouz, and Khalid Lamnawar*

ABSTRACT: The aim of the present work was to investigate a 3D manufacturing process dealing with 3D Direct Pellet multi-Extrusion (DPPmE). Throughout this paper, various functionally graded materials (FGM) were obtained with tailored properties for bone regeneration. Therefore, an experimental investigation was performed to gain a better understanding of the structure-processing-properties relationships. A poly(D,L-lactic acid) (PDLLA) matrix and bioglass (BG) or hydroxyapatite (HA) bioactive fillers were chosen to obtain hybrid FGM in comparison to composite references. Different compositions and shape factors (from microspheres to fibers) of these bioactive fillers were used to control the PDLLA matrix degradation. Then, different strategies of DPPmE were used to tailor and tune the desired gradient of properties. Interestingly, good interfaces and adhesion properties were obtained. Subsequently, rheological, size-exclusion chromatography, and porosity measurements corroborated the present findings. Besides, tensile as well as thermomechanical properties showed the advantages of the DPPmE process to fabricate FGM composites with tailored architectures.

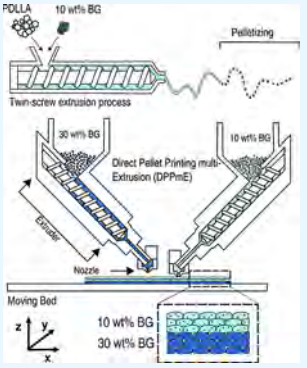

KEYWORDS: *3D printing, multifunctional composites, biocomposite, microstructural analysis, bioglass, rheology*

1. INTRODUCTION

The number of internal fixation surgeries continues to increase year by year.[1] To improve patient post-healing and avoid a second surgical intervention to remove the bone implant, numerous studies have focused on the use of resorbable polymers,[2] ceramics,[3] and their composites.[4]

Poly(α-hydroxy ester) matrices, especially poly(L-lactic acid), poly(D-lactic acid), and their copolymer poly(D,L-lactic acid) (PDLLA), combined with bioactive fillers like bioglass (BG) or hydroxyapatite (HA) have been extensively studied for biomedical applications due to their biocompatibility, excellent mechanical properties, and controllable degradation rate.[5]

Bioglass (BG) and hydroxyapatite (HA) are inorganic osteoconductive fillers commonly used in composites for bone regeneration. BG improves both bone growth and differentiation. When BG is in contact with body fluids, a layer of HA develops on the BG surface, thus facilitating the attachment of osteoclasts and the proliferation of osteoblasts.[6]

When it comes to obtain fully dense parts, two different ways of processing poly(α-hydroxy ester)/BG composites are differentiated in the literature: solvent casting[7] and molten manufacturing techniques (e.g., injection[8] and compression molding[9]). The first route involves the use of toxic and costly solvents as well as energy for solvent evaporation and recycling. However, various authors have observed that in the presence of BG high-temperature processing of poly(α-hydroxy ester) can cause a significant reduction of the polymers' molecular weight and mechanical properties.[10] In our previous studies, we described how the characteristics of BG affected the degradation reaction between PDLLA and BG.[8] We demonstrated that the thermal treatment, composition, and content of BG or the extrusion temperature could reduce the hydrolytic degradation of PDLLA during the thermal processing. Compared to the 45S5 composition (45 wt % SiO_2; 24.5 wt % CaO; 6 wt % P_2O_5; 24.5 wt % NaO_2), BG containing a lower amount of sodium and phosphate in its composition may exhibit a lower matrix degradation during the manufacturing step.[11] Hence, in order to minimize the degradation, a less reactive BG has to be chosen.[12]

On the one hand, innovative manufacturing processes like fused deposition modeling, electrospinning, or robocasting open up new possibilities to fabricate orthopedic implants based on biomaterials with an adjustable functional gradient. These systems, commonly named functionally graded materials (FGM), exhibit a structure and/or composition that gradually change in a particular direction with tailored properties. Functional gradient can be adapted to achieve a suitable

Received: August 23, 2022
Accepted: December 19, 2022

Table 1. Properties of Bioactive Fillers

name	nature	ρ(g/cm^3)	d_{50}(μm)	diameter-length(μm)	specific surface area (m^2/g)
HA	HA	3.14	20	-	9.5×10^{-1}
BG-MS	S53P4	2.64	60	-	3.8×10^{-2}
BG-fibers	S53P4	2.64	-	7−120	2.3×10^{-1}

structural strength, surface roughness, or induce bioactive, anti-inflammatory antibacterial response during implantation.[13] There exist several techniques in the literature to produce graded coatings (FGC),[14,15] FGM with a gradient in porosity[16−19] and 3D graded parts for orthopedic applications.[20] Through the last years, only few authors presented the possibilities of resorbable poly(α-hydroxy ester)/bioactive fillers in FGM composites for bone tissue engineering applications. For example, Eqtesadi & Motealleh[14,15] improved the mechanical properties of 45S5 bioglass robocast scaffolds by applying a PLA coating. Mehboob[21] proposed a design based on finite element analysis of a FGM composite to resist the different stresses during the healing of bone fractures. They also studied the mechanical properties evolution of a multilayer FGM composites fabricated by hot-pressing immersed in a phosphate-buffers saline (PBS) solution.[20] Masoudi et al.,[22] fabricated a bilayered membrane by electrospining to combine guided bone and guided tissue regeneration properties. Moreover, Ma et al.,[23] presented an in vivo study of FGM with tailored mechanical properties and bioactivity of orthopedic implants fabricated by solvent casting. The principal current technologies to manufacture the FGM in the literature are freeze-drying, electrospinning, solvent coating, solvent assembling, hot-pressing, and 3D printing extrusion. However, the studies of FGM fabricated by 3D printing are focused on scaffolds with a gradient in porosity to limit the stress-shielding effect or/and with a high porous connectivity to facilitate the fluid flow through the implant.[13]

Besides, preceding work[24] has shown that after only 14 days of in vitro tests, the mechanical properties of the composite decreased by 60%. The mechanical and morphological properties of neat PDLLA specimens remained stable for 6 months of immersion in a phosphate-buffered saline solution (commonly used in biological degradation simulation). Therefore, FGM PDLLA/BG and/or PDLLA/HA with different bioactive filler content may exhibit bioactivity and ensure the resistance during a long in vitro immersion period.

On the other hand, additive manufacturing techniques present several strengths like rapid fabrication, customization, and substantial saving material. Further advantages of this manufacturing technology are that the porosity and mechanical properties of the final parts can be adjusted to respond the specifications of different medical devices. 3D Direct Pellet multi-Extrusion (DPPmE) is a Fused Deposition Modeling (FDM) technique based on an extrusion system using polymer pellets as the starting material and thus avoiding the filament preparation required for Fused Filament Fabrication (FFF). This technique democratizes the access to additive manufacturing techniques since it expands the applicability of FDM to non-commercial materials in the filament form.[25−27] In former studies, it has already been demonstrated that well-designed structures can be manufactured with thermal unstable polymers[28] and mechanical properties comparable to those of injection-molded parts.[29] Besides, it is necessary to pay special attention to control the rheological properties of molten materials (like viscosity modulus, zero-shear viscosity, or relaxation time/elasticity) during extrusion through the nozzle and after deposition in order to ensure good interlayer welding and the mechanical robustness of 3D-printed parts.[30,31] Further, some DPPmE systems present an extrusion system with multiple screws, resulting in FGM-printed parts with different material composition and architecture. In a previous study of our team, we probed the successful control of the interfacial bonding of multimaterial systems fabricated by this technique.[32,33] Despite the interesting papers dedicated in the recent years to 3D printing process (specially to FDM[34]), there is an aperture to DPPmE and its adaptation to develop innovative FGM devices for medical applications.

In this work, three types of fillers, HA microspheres, BG microspheres, and BG fibers, were used to illustrate how the content, shape, and nature of the fillers affected the morphology, rheology, and mechanical properties of PDLLA composites. Moreover, the 3D printing of dense FGM parts was carried out with special attention to the printing temperature to ensure a rather constant viscosity and minimize the matrix degradation during processing. To conclude, we present the post-fabrication mechanical properties of multi-component specimens with different bioactive filler contents to show the potential application of 3D DPPmE FGM for load-bearing orthopedic implants.

2. EXPERIMENTAL SECTION

2.1. Materials and Manufacturing Process. *2.1.1. Materials.* An amorphous poly(D,L-lactide), hereafter referred to as PDLLA (4060D, Nature Works LLC, USA) (~10 €/kg), with 19.5% level of D isomer and a density of 1.24 g cm^{-3} was used in this work as it exhibited similar properties to the medical grade PDLLA R207S (Evonik, USA) (~6000 €/kg). PDLLA presented a weight average molar mass $\bar{M}_w$ = 136 kg mol^{-1}, a number average molar mass $\bar{M}_n$ = 94 kg mol^{-1} and a polydispersity $Đ_M$ = 1.4 obtained by SEC measurements in chloroform. Rheological and molar mass details of R207S are given in Supporting Information A. Before extrusion and granulation, PDLLA was dried for 4 h at 45 °C under vacuum to prevent hydrolytic degradation during the processing.

Particles of antibacterial bioactive glass S53P4 (BG) (XL-Sci Tech, USA) with a chemical composition of 53 wt % SiO_2; 20 wt % CaO; 4 wt % P_2O_5; 23 wt % NaO_2, as well as particles of hydroxyapatite (HA) (Plasma Biotal, UK), were mixed with PDLLA.[35] For BG, two different particle shapes were used: microspheres and fibers. HA microsphere fillers are used as a reference (no chemical interaction between HA and PDLLA is mentioned in the literature). Table 1 summarizes the main properties of bioactive fillers. Before compounding, HA and BG powders were dried for 4 h at 150 °C under vacuum.

2.1.2. Compounding and Pelletizing of Filled PDLLA. Compounding of the composite was carried out in a Haake Minilab Rheomax CTW5 Mixing (Thermo Fisher Scientific, Cleveland, OH, USA) with a filling volume of 7 cm^3 at a temperature of 150 °C and a rotor speed of 40 rpm. The compounder can be used as an extruder or mixer since it combines a twin-screw extruder with a back-flow channel. Since no recirculation was used in this study, a short residence (~30 s) and a mixing volume of 5.5 cm^3 were fixed. PDLLA powders micronized by Micronis (Colayrac-Saint-Cyrq, France) with d_{50} = 200 μm were blended independently with BG and HA particles

at a total filler content of 0, 10, or 30 wt % (corresponding to 0, 5.2, or 17.5 vol % BG and 0, 4.2, or 14.4 vol % HA, respectively). Subsequently, the extrusion filament was cut into pellets using a mechanical granulation machine. The compounding and 3D printing steps were made in a white room. The pellets were then dried for 4 h at 45 °C under vacuum and stored in sealed desiccators with silica gel until the 3D printing fabrication.

2.1.3. Direct Pellet Printing Multi-Extrusion (DPPmE). A PAM Series Lx (Pollen AM, France) printer with four screw-based extruders was used to prepare mono- and multicomponent tensile parts. As shown in Figure 1, the specimens were fabricated by filament deposition layer-by-layer system using a single-screw extruder fed directly with composite pellets.[36]

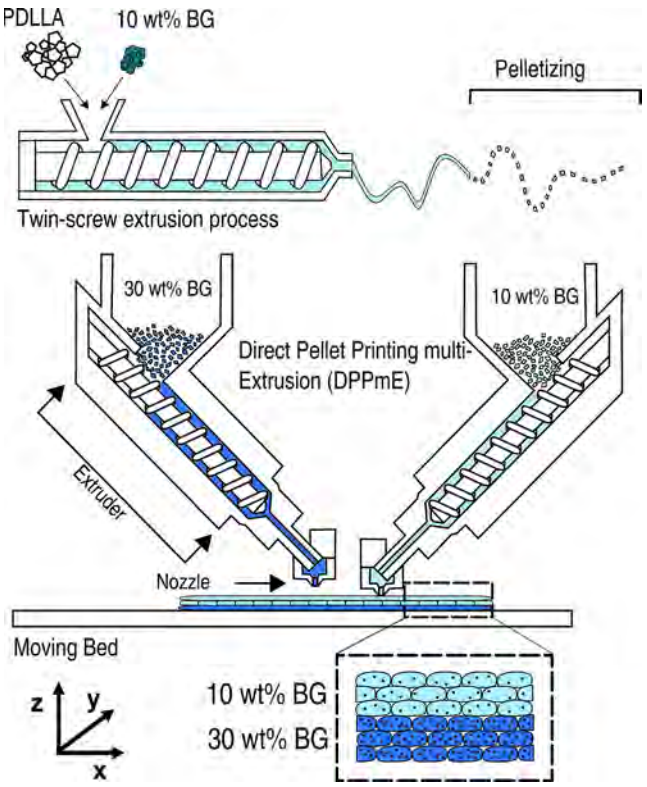

Figure 1. Schematic representation of an example of (top) the composite fabrication and (bottom) the direct pellet printing multi-extrusion process (DPPmE) with 10 and 30 wt % of BG.

All of the samples were printed using a nozzle size of 0.4 mm, a −45°/45° orientation with a layer thickness of 0.2 mm, a filament width of 0.4 mm, and a printing speed of 30 mm/s inside an enclosed temperature-controlled chamber in a white room environment. For the clarity of this study, only results with this speed will be presented. The bed temperature was set at 55 °C. For PDLLA/BG, the printing temperature was set at 160 °C for the extruder and 170 °C for the nozzle. For the PDLLA and PDLLA-HA composites, the temperature was set at 180 and 190 °C, respectively. The different FGM configurations (strategy I, II, and III) studied in this work are shown in Figure 2. Prior to printing, a skirt was printed around the sample to normalize the flow. For multicomponent systems, the polymer in the nozzle was renewed by printing a volume support. The total printing time for the tensile samples was 215 s for strategy I. Before printing the new sample, the remaining melt was extruded in order to remove the composite material from inside the screw. The main objective is to avoid thermal degradation of the residual materials.

Five replicas were printed for each strategy. For the clarity purpose, only results with the same filler nature will be shown for each architecture.

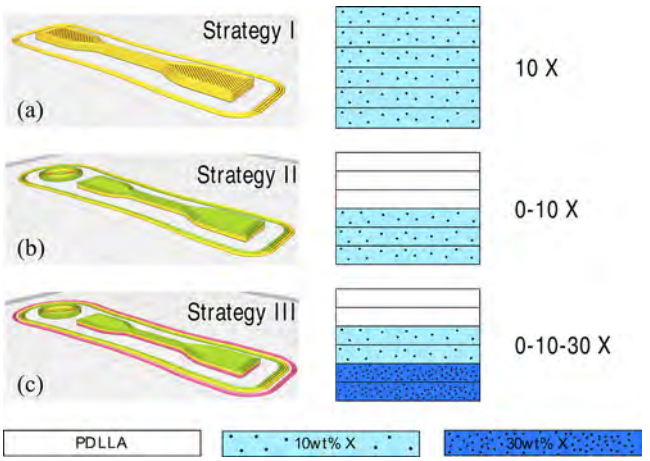

Figure 2. Tensile sample model from a 3D printing software (CURA, Ultimaker) for (a) strategy I, (b) strategy II, and (c) strategy III to print FGM composites with the corresponding layer configurations. X represents the bioactive filler (BG or HA).

2.1.4. Injection Molding. Tensile dumbbell-shaped bars were prepared on a HAAKE Minijet injection molder (Thermo Fisher Scientific, Cleveland, OH, USA). The injection molding (IM) procedure involved a cylinder temperature at 180 °C and a mold temperature at 55 °C under 800 bar of pressure for 20 s. The tensile tests of dumbbell-shaped fabricated by IM were used as a reference to compare with the mechanical properties of strategy I DPPmE.

2.2. Methods. *2.2.1. Rheological Analysis in the Linear Viscoelastic Regime.* Rheological measurements in small amplitude oscillatory shear (SAOS) were performed with a DHR-2 (TA Instruments, USA) stress-controlled rheometer using a parallel-plate geometry (ϕ = 25 mm, gap distance 1.2 mm). Sample discs were prepared by hot pressing at 140 °C for 2 min at 40 bars to minimize matrix degradation.[37] Dynamic time (at 1 rad•s^{-1}) and dynamic frequency sweep (from 628 to 0.1 rad•s^{-1}) measurements in the linear viscoelastic regime were carried out at temperatures corresponding to those in the extruder (160 °C/180 °C) and nozzle (170 °C/190 °C) of DPPmE, respectively, under a continuous nitrogen purge. The LVE characterization is given in Supporting Information.

2.2.2. Size-Exclusion Chromatography (SEC) Analysis. The average molar mass in weight and number, $\bar{M}_w$ and $\bar{M}_n$ of PDLLA before and after processing of composites was determined by size-exclusion chromatography (SEC) in chloroform solvent using a tetra detection system equipped with a Schimadzu SPD 20A (λ = 280 nm), a Wyatt TREOS (3 angles), a ViscoStar II Wyatt and a Schimadzu RID 10A. The SEC system had three columns (PL gel 5 μm Mixed C 300 × 7.5 mm, polystyrene/divinylbenzene), and the analysis temperature was 30 °C. The dn/dc used for PDLLA in chloroform was 0.023, and the concentration of the samples was 3 mg/mL.[38] Before the SEC analysis, the solutions were filtered with 0.45 μm filters to remove the BG and HA particles.

2.2.3. Archimedes Method. The procedure based on the Archimedes method was applied to measure the porosity of different printed parts.[39] A Mettler AE100 (Mettler-Toledo Inc., Columbus, OH) analytical balance with a capacity of 100 g and an accuracy of ±0.01 mg was used for the mass measurements.

According to Archimedes' principle and by not considering the open cavities, the density can be calculated as follows

$$\rho_{sample} = m_{air}\frac{\rho_{liquid}}{m_{air} - m_{liquid}} \quad (1)$$

Here, ρ_{sample} is the measured sample density (g cm^{-3}), ρ_{liquid} is the density of the ultra-purified water at room temperature (g cm^{-3}), m_{air} is the mass of the sample in air (g) and m_{liquid} is the mass of the sample in ultra-purified water (g).

Finally, the porosity rate of the samples was calculated according to

$$\%\text{porosity} = \left(1 - \frac{\rho_{\text{sample}}}{\rho_{\text{theoretical}}}\right) \times 100 \quad (2)$$

where $\rho_{\text{theoretical}}$ is the actual density of the composite calculated from additive law ($\rho_{\text{theoretical}} = \sum p_i \phi_i$, with p_i and ϕ_i the density and volumetric fraction of each component).

2.2.4. X-Ray Tomography. X-ray tomography measurements were conducted using a laboratory X-ray source on an EasyTom tomograph (RX Solutions, France) at high resolution with a 1.5 μm voxel size on small samples (~1.5 × 1 × 1 mm). This tomograph was equipped with an LaB6 emission tip for the X-ray source, which ensured that the actual spot size was physically smaller than 1.5 μm. This way, the resolution did not become modified by geometric blur. All the data were reconstructed by a filtered back-projection Feldkamp algorithm.

2.2.5. Scanning Electron Microscopy (SEM) Analysis. SEM micrographs were taken on uncoated samples using a Supra 55 microscope (Zeiss, Oberkochen, Germany). The specimens were first cryo-fractured in liquid nitrogen and then observed at low acceleration voltage (1 kV) under high vacuum mode.

2.2.6. Mechanical and Thermomechanical Characterization.

2.2.6.1. Tensile Testing. In accordance with ASTM D638, tensile tests were performed on dumbbell-shaped bars with dimensions of l_0 = 20 mm, b = 4.2 mm, and h = 1.2 mm for DPPmE and l_0 = 20 mm, b = 4.2 mm, and h = 2 mm for IM parts. The measurements were conducted on a universal AGSX 5 kN (Shimadzu Corporation, Ltd., Kyoto, Japan) tensile tester with a crosshead speed of 1 mm/min.

2.2.6.2. Dynamic Mechanical Analysis (DMA). DMA analysis was performed on hot-pressed and 3D-printed rectangular samples (h = 0.6 mm, b = 4.5 mm, and l = 12 mm). Temperature sweep tests were carried out on a DMA Q800 (TA Instruments, USA) in tensile mode at a frequency of 1 Hz and a strain of 0.05%. Storage and loss moduli were determined as functions of temperature from 30 to 120 °C at a heating rate of 2 °C/min.

3. RESULTS

3.1. Dispersion and Microstructural Properties of 3D-Printed Filled Composites (Strategy I). The purpose of this section is to investigate the dispersion properties of BG and HA fillers in PDLLA matrix after compounding and 3D printing. Micro-computed tomography (μCT) and SEM analysis were therefore used to analyze the filler dispersion in the PDLLA matrix. The filler content of each specimen was calculated by image analysis using ImageJ. As shown in Table 2, the printed parts presented a slight difference between the compounding filler content and that calculated by ImageJ from the printed parts. For the following section, we have considered the value of the filler content as calculated from the image analysis of the printing parts. The mean values of porosity were measured by Archimedes' method. Interestingly, and according to the porosity study, the specimens of different filler content and nature had a very low porosity (between 1 and 3%).

Table 2. Quantified Porosity and Filler Content of Strategy I[a]

sample	wt %	$\rho_{\text{theoretical}}$(gcm^{-3})	ρ(gcm^{-3})	%porosity
PDLLA	0	1.24	1.22	1.7
PDLLA10-HA	13	1.35	1.28	2.8
PDLLA30-HA	28	1.49	1.47	1.1
PDLLA10-BG-MS	13	1.33	1.26	3.1
PDLLA30-BG-MS	25	1.39	1.36	2.2
PDLLA10-BG-fibers	7.0	1.28	1.23	1.8
PDLLA30-BG-fibers	25	1.46	1.36	1.7

[a]With an error bar of its standard deviation for theoretical density, experimental density and porosity (i.e., 0.03% and 0.1% respectively) and 1%, for wt %.

3.1.1. Particle Dispersion and Anisotropy from μCT Analysis. Two methods were employed to quantify the particle dispersion from μCT images: the free-space length (L_f)[40] and the degree of anisotropy[41] (DA) technique. Both procedures quantified the particle dispersion in the matrix by taking into account the effect of particle size, their content and facilitated the detection of possible defaults during the 3D printing process such as particle aggregation and internal porosity.

The free-space length (L_f) has been described by Khare et al.[40] as the length of the largest observation volume for which the most probable number of contained particles is zero.[40] As L_f is rather equal to the theoretical free space length of the Poisson distribution (L_p) (i.e., a completely random distribution of particles into the matrix) for the different composites presented in this study, we considered that the particles were dispersed homogeneously. As previously described, the L_f method gives quantitative information of the level of particle dispersion. Although L_f can be calculated for fibres, this technique is more appropriate for calculating the dispersion of spherical particles in the matrix. Moreover, the DA value, with [0,1] boundaries (0 means the dispersion is completely isotropic and 1 extremely orientation in the structure), was used to describe the type of particle orientation as well as the organization using the plugin of ImageJ namely "BoneJ".[41,42] Therefore, the DA was calculated from the radius of the ellipsoid (D1, D2, and D3) fitted with the mean intercept length (MIL vectors) points as

$$\text{DA} = 1 - \frac{1}{R_z^2} / \frac{1}{R_x^2} \quad (4)$$

with $R_z > R_y > R_x$.

Table 3 summarizes the obtained DA results from the printed parts and the particle dispersion properties in the printed parts (Lf and Lp). Furthermore, Figure 3a and 3b illustrates the 3D BG-fibres and BG-MS dispersion with 10 wt % in the PDLLA matrix, respectively. BG fibres form an orthotropic structure (i.e., a planar alignment particle on the plane perpendicular to the Z direction), whereas BG microspheres present a homogeneous dispersion. The radius of the ellipsoid in the printing plane was longer than the length in the Z direction ($R_z < R_x R_y$) and as a result, the filament extrusion induced an alignment of BG fibres in the direction parallel to the nozzle. In the case of the microspheres, the distribution can be considered as completely random (DA~ 0).[41]

Table 3. Quantified Dispersions With the Free-Space Length and MIL Vectors

sample	L_f	L_p	DA	R_x	R_y	R_z
PDLLA10-HA	42	52.69	0.06	6.7	6.7	6.6
PDLLA30-HA	34	35	0.06	10.5	10.0	10.0
PDLLA10-BG-MS	50	56	0.14	5.7	5.4	5.3
PDLLA30-BG-MS	42	48	0.08	4.5	4.4	4.3
PDLLA10-BG-fibers	105	65	0.39	8.2	7.9	6.3
PDLLA30-BG-fibers	60	41	0.37	7.3	7.1	5.8

3.1.2. Microstructural Analysis of Printed Composites. Figure 4 shows the cross-section of strategy I for BG-MS, BG-fibers, and HA fillers. PDLLA/BG and PDLLA/HA printed

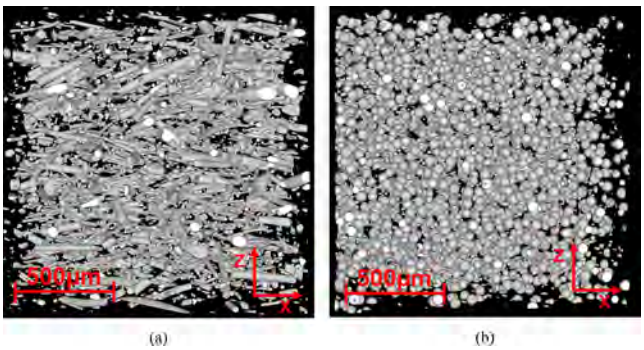

Figure 3. 3D structure of the printed composite reconstructed from μCT images (matrix hidden) for (a) PDLLA-10-BG-fibers and (b) PDLLA-10-BG-MS.

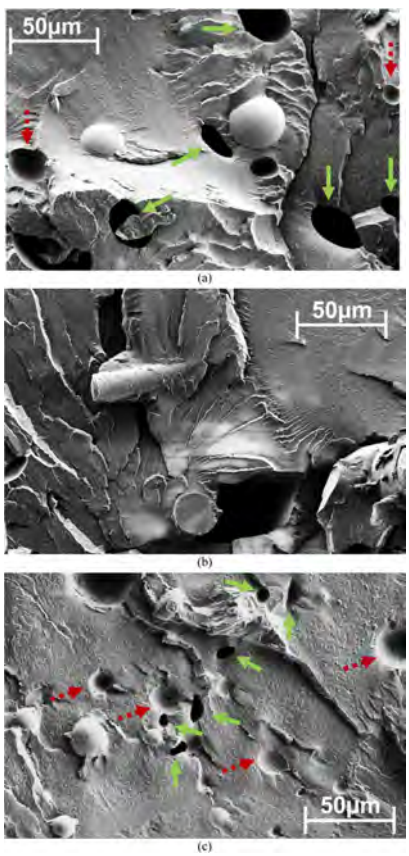

Figure 4. Scanning electron micrograph of cryo-fractured cross sections of strategy I composites (a) PDLLA-10-BG-MS, (b) PDLLA-10-BG-fibers, and (c) PDLLA-10-HA. Red dashed arrows represent the hole of particle loosening and green solid the smaller pores inside the filament.

samples exhibited good particle/matrix wetting, with the presence of intra-filament pores (between 10 and 25 μm), which are specific to composite parts fabricated by a 3D printing extrusion process.[43] However, as indicated with red dashed arrows in Figure 4a,c, the BG and HA particles presented a loosening owing to a low adhesion with the surrounding PDLLA. HA and BG particles showed the same behavior: good wetting of particles by the PDLLA matrix with poor adhesion.

3.2. Investigation of Melt Rheological Properties of Filled PDLLA Materials. 3D printing involving material extrusion in the molten state can induce some polymer degradation. The choice of printing parameters must strike a balance between reducing this degradation, ensuring good welding between adjacent printed filaments, and avoiding the maximum torque limits of the screw-extrusion of DPPmE. The 3D-printing extrusion process conditions were optimized by a rheological characterization in the linear viscoelastic (LVE) domain. As observed in our previous works,[8] the degradation kinetics of PDLLA is influenced by the presence of BG fillers. Indeed, in the molten state, the presence of BG increases the polymer degradation since the R-Si-O- on the surface of BG catalyzed the ester bond scission of PDLA chains.[8] Figure 5 shows the thermal stability investigated by analyzing the evolution of the relative viscosity (η_r) (Equation 3).

$$\eta_r(t) = \frac{\eta^*(t)}{\eta^*(t=0)} \quad (3)$$

PDLLA and PDLLA-HA (Figure 5a) composites showed a slight decrease in the relative viscosity due to the hydrolytic degradation of PDLLA.[44] Interestingly, HA fillers on PDLLA-HA composites seem to reduce the hydrolytic degradation since they can absorb the remaining moisture enclosed into the matrix. However, compared with PDLLA and PDLLA-HA, the BG-based composites presented a higher continuous decrease of the relative viscosity over time.

Figures 5b and 5c show that, by reducing the temperature of the thermal stability test from 180 to 160 °C, the PDLLA-BG composite yielded a smaller decrease of η_r. Therefore, the extruder temperature of DPPmE was set to 160 °C for BG composites in order to reduce the polymer degradation during the 3D printing process. Moreover, η_r was also affected by the filler content and shape of the BG particles (e.g., with 30 wt %, the viscosity decreased faster than with 10 wt % of BG). Finally, owing to the high specific surface of BG fibers, composites filled with BG fibers presented a higher decrease in relative viscosity compared to those filled with microspheres (MS). Based on the obtained results, it is really clear that it is possible to decrease the degradation amount of the PDLLA matrix by reducing the printing temperature and decreasing the surface contact of BG with the PDLLA matrix. Figure 5d presents an overview of the complex viscosity modulus of neat PDLLA and its filled composites with HA and BG-MS as a function of the angular frequency. Interestingly, by reducing the printing temperature of PDLLA/BG composites up to 20 °C, we were able to limit the matrix degradation and achieve a similar viscosity to neat PDLLA at 190 °C.

3.3. Investigation of the Filler Effect and FGM Structure. *3.3.1. Microstructural Analysis of Printed Multicomponent FGM (Strategy II and III).* Figure 6 shows the cross-section of FGM multicomponent with strategy II (0−10 BG-fibers) and strategy III (0-10-30 HA). They exhibit the two examples of interface adhesion between different components and layers. In some cases, SEM images of multicomponent systems presented almost any porosity between layers and filaments (Figure 6a), whereas other samples exhibited inter-filament pores (50−100 μm) (Figure 6b). Interestingly, specimens fabricated following strategies II and III showed good interface adhesion, regardless of the filler content of the adjacent layers. Hence, the optimization of processing parameters (e.g., printing temperature, printing speed, infill density, or infill pattern) made it possible to achieve systems

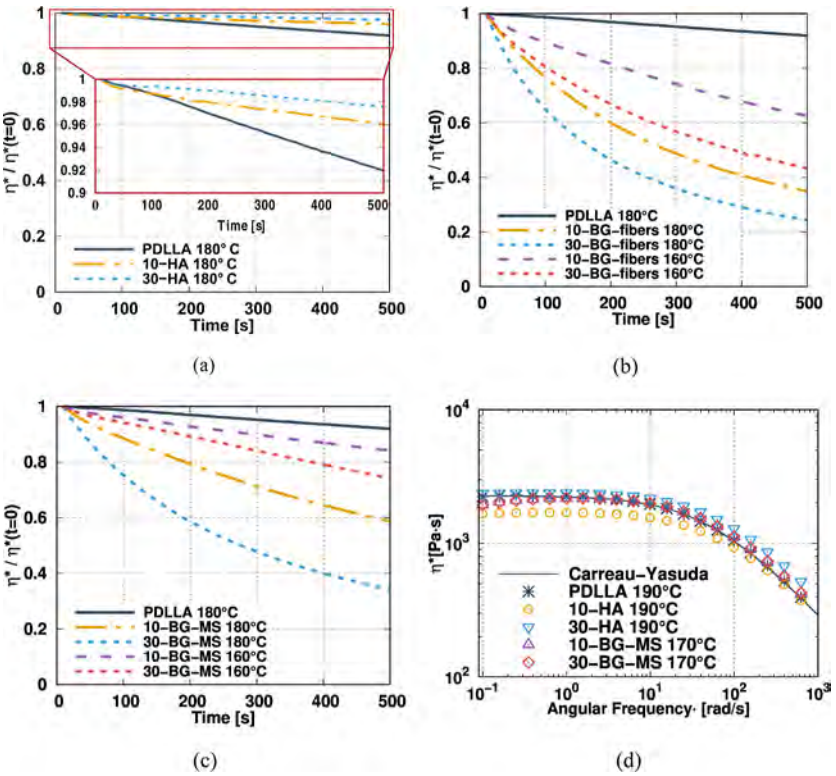

Figure 5. Time evolution of the relative viscosity at 1 rad/s of (a) HA-based composites at 180 °C; (b) BG-fiber-based composites at 160 and 180 °C; (c) BG-MS-based composites at 160 and 180 °C; (d) example of the complex viscosity modulus as a function of the angular frequency of neat PDLLA, PDLLA/HA, and PDLLA/BG-MS composites at the corresponding nozzle temperatures with the Carreau-Yasuda model fitting of PDLLA.

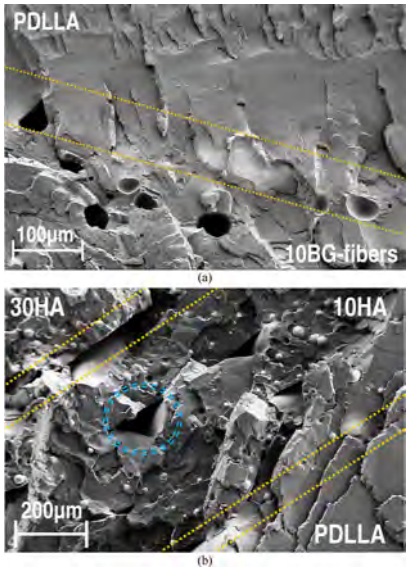

Figure 6. Scanning electron micrograph of cryo-fractured cross sections of the composites taken in the bulk of FGM (a) PDLLA-0-10 BG fibers and (b) PDLLA-0-10−30 HA. Blue solid circle represents the pore between the filaments and the yellow dashed line the interface between different components.

with no visual interface or delamination between different layers.

3.3.2. Effect of Filler and DPPmE on the Molar Mass of PDLLA. The average molecular weight values of the pellets and specimens were measured by size exclusion chromatography (SEC). The $\bar{M}_w$ values of PDLLA extracted from the composites after the extrusion-compounding step and those of the PDLLA after the 3D printing are compared in Figure 7.

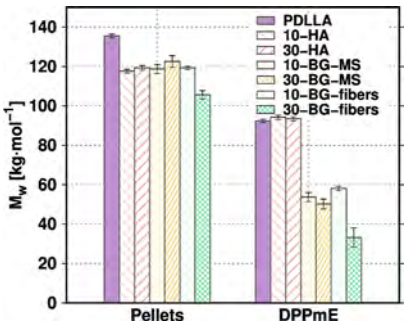

Figure 7. Evolution of the average molar mass ($\bar{M}_w$) for pellets and printed parts following strategy I with various biocompatible fillers.

A reduction of $\bar{M}_w$ revealed the occurrence of PDLLA degradation during the extrusion-pelletizing steps and the DPPmE process. This reduction in $\bar{M}_w$ after extrusion-pelletizing was similar for all composites except for the 30 wt % BG fibers, which presented a lower $\bar{M}_w$ value. As observed in our previous studies,[8] the addition of BG increased the matrix degradation, especially when the surface contact of PDLLA/BG was increased (high filler content or shape factor).

As shown in Figure 7, compared with the pellets, the PDLLA/BG specimens displayed a 50% reduction in $\bar{M}_w$. However, even if $\bar{M}_w$ decreased for the printed parts, the molecular weight remained constant for parts printed under

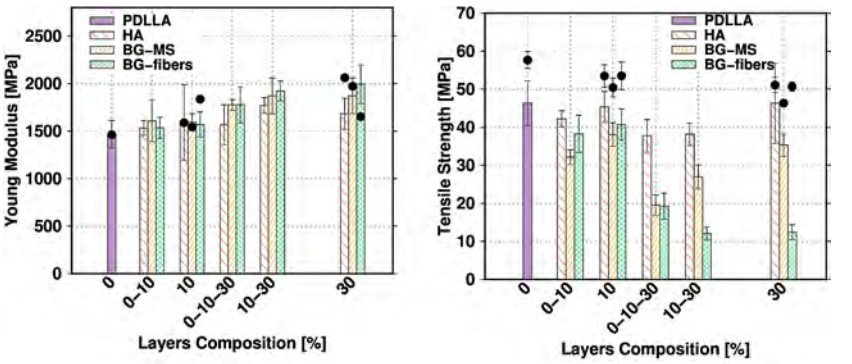

Figure 8. Evolution of (a) Et (MPa) and (b) σ_{max} (MPa) of composites based on HA, BG-MS, and BG-fibers with various filler content and multicomponent systems. The dots represent the values of injected parts with the same composition.

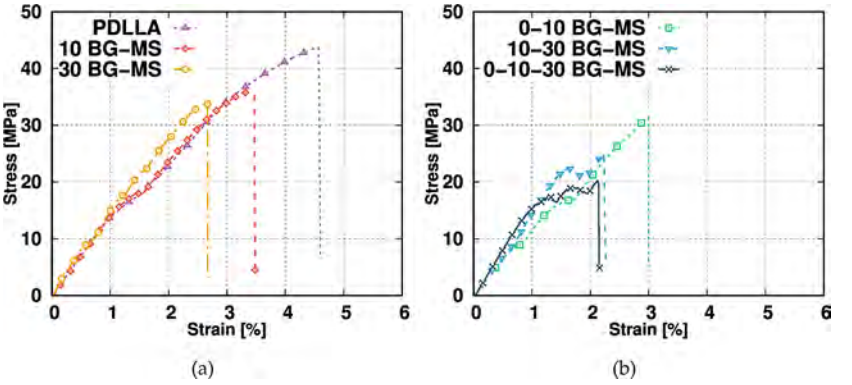

Figure 9. Stress−Strain of BG-MS 3D-printed FGM composites in (a) strategy I and (b) strategy II and III systems.

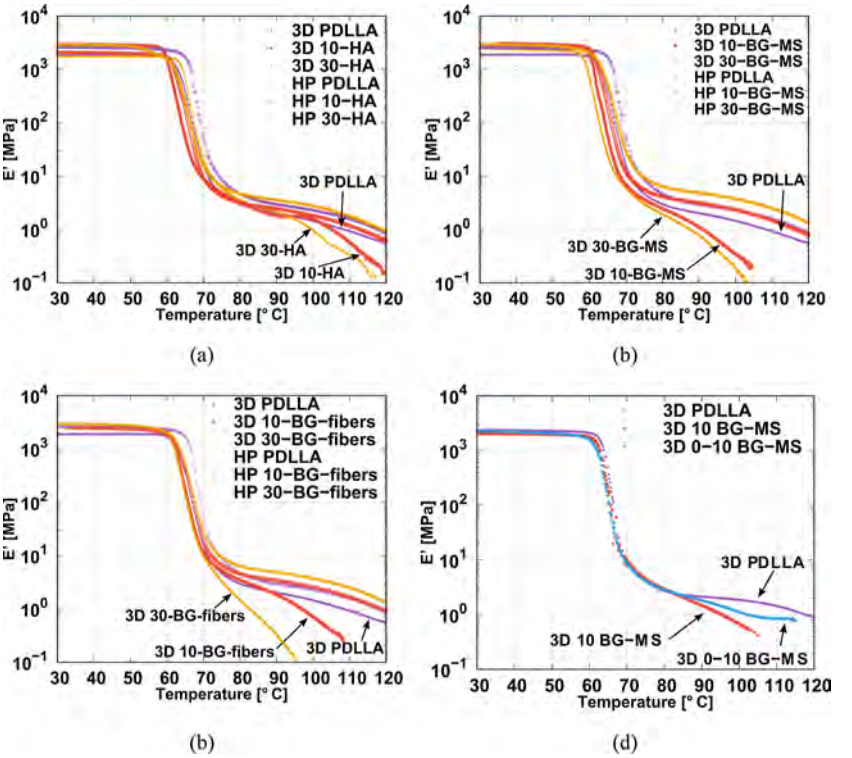

Figure 10. Evolution of *E'* (MPa) as a function of the temperature for DPPmE (3D) and hot-pressed (HP) samples of (a) HA, (b) BG-MS, (c) BG-fibers, and (d) for DPPmE PDLLA, 10-BG, and strategy II 0−10 BG-MS.

similar conditions, confirming a good repeatability of the process. This degradation was thus mainly due to the chemical reaction between PDLLA and BG in the molten state.

Interestingly, even at high filler contents, printed parts based on HA presented a value of $\bar{M}_w$ close to that of printed PDLLA, confirming a low interaction between HA and PDLLA. Thus, multicomponent FGM (strategy II and III) combine a bioactive composite with a component presenting a low matrix degradation after processing.

3.3.3. Mechanical and Thermomechanical Properties. *3.3.3.1. Tensile Testing.* Figure 8a,b displays the evolution of the tensile modulus (Et) and maximum tensile strength (σ_{max}) as functions of the filler contents and manufacturing strategy. Surprisingly, the Young moduli of the printed parts were close to those observed for injected parts with the same composition. Moreover, multicomponent specimens presented an intermediate modulus between the values of the different constitutive layers.

Furthermore, the tensile strength of strategy I systems was rather constant for almost all the different composites; only the one with 30 wt % of BG fibers presented a decreased strength (Figure 8b). However, compared to IM, DPPmE specimens exhibited a lower tensile strength. It seems that the residual stress and polymer chains orientation induced by the process in formers may enhance the tensile strength properties. FGM based on strategy II with HA or 0−10 BG fibers and MS displayed a tensile strength slightly lower than that observed for strategy I systems. However, FGM based on strategy II and III containing 30 wt % of BG exhibited a decreased tensile strength compared to the 0−10 assembly. Lap shear tests confirmed a good adhesion between different components as the fracture occurred in a stress concentration location instead of at the interface between different components (cf. Supporting Information B).

As can be seen in Figure 9a,b, a stress fluctuation occurred in the stress/strain curve, suggesting that micro-cracking took place on the interfaces during the tensile tests, thus initiating the breaking of the sample.[45,46] This fluctuation was more pronounced for multicomponent specimens, especially with a 0-10-30 configuration. Thus, even if we considered good interfacial adhesion between layers of different filler content, the layers presenting the worst mechanical properties promoted the fracture of the FGM specimens. For the clarity of this study, we show only the results with BG-MS on Figure 9 (since they show higher values of σ_{max} than BG-fibers).

3.3.3.2. Thermomechanical Properties and Validation of FGM Design. As shown in Figure 10, DPPmE and hot-pressed samples of each content and filler presented the same elastic modulus at a temperature below T_α (the temperature of α relaxation associated with the glass transition). The hot-pressed samples were prepared to eliminate any effect of orientation induced during IM parts. They showed the classical behavior of filled systems, that is, a higher plateau modulus in comparison with PDLLA when the filler content is increased. However, for the DPPmE specimens, the rubbery plateau displayed a shift to lower temperatures, and the length of the plateau was reduced for systems containing BG particles. In addition, highly filled systems presented an even shorter domain (e.g., samples with 30 wt % of BG-fibers did not show a plateau as the value of E' decreased continuously as a function of temperature). As a result, the shortening of the rubbery plateau highlighted the matrix degradation induced by the DPPmE process, whatever the nature of the filler.

Figure 10d shows an example of the thermomechanical properties of the 0−10 BG-MS configuration with the medical grade PDLLA matrix (R207S). The medical grade PDLLA and its composites presented a slightly longer rubbery plateau than the industrial grade PDLLA. Interestingly, the FGM with the 0−10 BG-MS configuration presented a rubbery plateau value in between the ones of its two own layers. Therefore, the thermomechanical properties of FGM were improved compared to 10-BG-MS while preserving the bioactive properties.

4. DISCUSSION

In this work, the evolution of the relative viscosity is a suitable tool to probe the thermal sensitivity of PDLLA and its filled~~filled~~ composites at the molten state and longer residence time, simulating the process conditions. In the case of the BG composites, the viscosity presented a significant decrease with time due to matrix degradation. At high temperatures, the silicate groups on the surface of the BG were associated with counterions and accelerated the PDLLA degradation.[8] Thus, the thermally induced PDLLA degradation could be limited by reducing the screw and nozzle temperatures for the PDLLA-BG composites. For PDLLA and the PDLLA/HA composites, the evolution of the relative viscosity reflected a higher thermal stability compared to PDLLA/BG composites. Moreover, SEC and DMA measurements confirmed the matrix degradation obtained by the rheological analysis.

Prior to printing, the melt in the extrusion zone was extruded in order to eliminate residual material which can be degraded with time. However, the rheological measurements highlighted the thermal instability of high-filled BG composites (30 wt %), and as a result, the BG specimens presented a more significant decrease in the molar mass of the matrix and a loss of mechanical properties. As observed by the SEC analysis, the molar mass was rather stable for successive printing, confirming the repeatability of the process with thermally unstable composites.

The microstructural analysis by SEM confirmed good particle-PDLLA wetting for the BG-fibers, the BG-MS, and the HA microspheres. Compared to HA, BG showed a better interaction with the matrix; a thin layer of PDLLA adhered to the surface of BG. This difference may be due to the chemical reaction described in our previous work.[8] The detection of filler detaching from the cryo-fractured cross-section of SEM confirmed a low adhesion with the surrounding PDLLA.

Analysis of the μ-CT images of printed parts revealed that DPPmE enabled a homogeneous distribution of the particles in the PDLLA matrix. For the microspherical fillers, the free space length (L_f) confirmed the good dispersion. Besides, for the fiber fillers, the degree of anisotropy indicated a particle alignment along the printing direction, which may induce an improvement of the mechanical properties on the beneficial orientation.[47] Even if, in general, the SEM images showed that the layers presented good interfacial adhesion; we observed a slight porosity (between 1 and 3%) after porosity measurements by Archimedes' method. In addition, the pores observed in the SEM micrographs, with a size between 10 and 100 μm, indicated a fluctuation of flow rate during the extrusion.

Compared to parts fabricated by injection molding, the presence of internal pores in the 3D-printed parts induced a decrease in tensile strength. Besides, the value of the standard deviation of mechanical properties was higher for the 3D-printed parts.

Interestingly, the thermomechanical properties of the hot-pressed PDLLA-BG composites presented the classical behavior of filled systems: the storage modulus increased for a higher filler content. However, the printed samples presented a decrease in E' and a shortening of the rubbery plateau, which indicated some degradation of the matrix. Thus, the pre-processing step of compounding had a smaller effect than the DPPmE process.

The second objective of this article was to study the possibilities of 3D-printed multicomponent parts with bioactive filler for load-bearing implants. First, multicomponent systems with two (strategy II) and three (strategy III) content types were more difficult to process as the thermal stability of more than one composite in different extruders needed to be controlled for alternative printing. As observed by SEM, an incomplete healing of the adjacent layers led to a visible interface between the two layers. However, the FGM interface exhibited good properties as for lap-shear on bicomponent 3D-printed parts, the fracture occurred in stress concentration location of bulk material (Supporting Information A). Tensile tests revealed that the printed FGM with a composition of 0-10-30 and 10−30 wt % of BG presented poor tensile strength, whereas samples with the same composition of HA showed a behavior close to that of systems printed with strategy I. The fracture mechanisms of PDLLA/BG and PDLLA/HA composites were driven by the micro-cavitation and particle debonding.

Furthermore, system manufactured following the strategy II with 0−10 wt % (even BG or HA) presented good mechanical properties. Dynamic mechanical analysis revealed that the FGM strategy increased the thermomechanical properties since the rubbery plateau displayed a behavior between the 3D-printed PDLLA and the 10 BG-MS. Hence, the strategy II systems containing 0−10 wt % of BG seemed to introduce a different approach for the fabrication of FGM by 3D printing, as they contained a bioactive layer and a layer with a low-degraded matrix. Otherwise, the presence of HA in hybrid HA/BG FGM composites seems to play an interesting role to balance mechanical properties. The printed PDLLA layers played a role of mechanical support for the bioactive PDLLA-BG layers.

5. CONCLUSIONS

The aim of this work was to study the rheological, microstructural, and mechanical properties of PDLLA-BG and PDLLA-HA composites when processed by DPPmE multi-screw extrusion. This innovative manufacturing technique presented the advantage of producing functionally graded materials (FGM) with tailored properties for bone regeneration.

First, a significant influence of the processing temperature was detected by rheological analysis. Indeed, the molar mass measured by SEC revealed that DDPmE caused significant polymer degradation due to the chemical reactions of BG and HA. Thus, in order to assure a repeatability of the final properties and reduce the polymer degradation, the residence time and temperature of PDLLA in the extrusion mechanism had to be controlled.

Microspheres and fibres fillers were used to create a system presenting bioactive and mechanical properties.

The HA and BG fillers were homogeneously distributed within the PDLLA matrix in 3D printed systems as confirmed by SEM and μ-CT analyses. The filler particles exhibited a good wetting with the surrounding matrix. Interestingly, the non-detection of an interface between adjacent layers of systems based on strategies I, II, and III by SEM analysis confirmed solid welding during 3D DPPmE. Moreover, they presented low internal porosity. The addition of BG reduced the tensile strength of the composite and increased the Young modulus. Besides, the addition of HA did not lead to a notable impact on the mechanical properties. Although the tensile strength of the systems fabricated with strategies II and III was slightly lower when compared with the respective composites, we believe that the combination of BG and HA layers of different content will, under in vivo conditions, present good bioactivity and a higher mechanical resistance during implantation.

Finally, this study showed the potential of DPPmE multi-extrusion for the manufacturing of orthopaedic implants with bioactive fillers while assuring good mechanical properties and complex geometries. Even if the effect of hydrolytic degradation of PDLLA matrix in the molten state was minimized by the experimental protocol, the contact of BG fillers with PDLLA still influenced the molar masses of PDLLA at high processing temperatures. Hence, the authors believe that FGM combining a low-degraded (with HA fillers) and a bioactive layer (with BG fillers) is a key to tune the bioactivity during in vivo implantation. Further investigations of FGM systems based on PDLLA and bioactive fillers immersed in phosphate-buffered saline (PBS) solution will be performed to study the evolution of the morphological, microstructural, and mechanical properties of systems produced by DPPmE.

■ ASSOCIATED CONTENT

Supporting Information

The Supporting Information is available free of charge at https://pubs.acs.org/doi/10.1021/acsapm.2c01475.

Comparison between the physico-chemical properties of industrial and medical grade PDLLA, lap-shear results, FTIR spectroscopy to describe the degradation mechanisms, rheological investigation of the linear viscoelastic regime, and additional data of mechanical and thermomechanical properties of DPPmE parts (PDF)

■ AUTHOR INFORMATION

Corresponding Authors

Jean-Marc Chenal − *Université de Lyon, CNRS, UMR 5510, MATEIS, INSA-Lyon, Villeurbanne F-69621, France*; Email: jean-marc.chenal@insa-lyon.fr

Khalid Lamnawar − *Université de Lyon, CNRS, UMR 5223, Ingénierie des Matériaux Polymères, INSA Lyon, Université Claude Bernard Lyon 1, Université Jean Monnet, Villeurbanne 69621, France*; orcid.org/0000-0003-4907-0977; Email: khalid.lamnawar@insa-lyon.fr

Authors

Xavier Lacambra Andreu − *Université de Lyon, CNRS, UMR 5223, Ingénierie des Matériaux Polymères, INSA Lyon, Université Claude Bernard Lyon 1, Université Jean Monnet, Villeurbanne 69621, France; Université de Lyon, CNRS, UMR 5510, MATEIS, INSA-Lyon, Villeurbanne F-69621, France; Hassan II Academy of Science and Technology, Rabat 10100, Morocco*

Abderrahim Maazouz − *Université de Lyon, CNRS, UMR 5223, Ingénierie des Matériaux Polymères, INSA Lyon,*

Université Claude Bernard Lyon 1, Université Jean Monnet, Villeurbanne 69621, France; Hassan II Academy of Science and Technology, Rabat 10100, Morocco

Complete contact information is available at: https://pubs.acs.org/10.1021/acsapm.2c01475

Author Contributions

The manuscript was written through contributions of all authors. All authors have given their approval to the final version of the manuscript.

Funding

This work was supported by "Ministère de l'enseignement supérieur, de la recherche et de l'innovation, MESRI-France".

Notes

The authors declare no competing financial interest.

■ ACKNOWLEDGMENTS

X.L. would like to thank French government and INSA Lyon for financial support of his PhD studies. All the authors gratefully acknowledge Jérôme Adrien (MATEIS) for the tomography analyses, Dr. Xavier Morelle (IMP) for the fruitful discussions regarding the lap-shear results, and wish to thank the Liquid Chromatography Characterization Polymer Center of Institut de Chimie de Lyon (Agnes Crepet, IMP) for assistance and access to the SEC facilities.

■ REFERENCES

(1) Haglin, J. M.; Eltorai, A. E. M.; Gil, J. A.; Marcaccio, S. E.; Botero-Hincapie, J.; Daniels, A. H. Patient-Specific Orthopaedic Implants. *Orthop. Surg.* **2016**, *8*, 417−424.

(2) Kashirina, A.; Yao, Y.; Liu, Y.; Leng, J. Biopolymers as Bone Substitutes: A Review. *Biomater. Sci.* **2019**, *7*, 3961−3983.

(3) Baino, F.; Hamzehlou, S.; Kargozar, S.Bioactive Glasses: Where Are We and Where Are We Going?. *J. Funct. Biomater.***2018**, *9*(). DOI: 10.3390/jfb9010025.

(4) Gritsch, L.; Perrin, E.; Chenal, J. M.; Fredholm, Y.; Maçon, A. L.; Chevalier, J.; Boccaccini, A. R. Combining Bioresorbable Polyesters and Bioactive Glasses: Orthopedic Applications of Composite Implants and Bone Tissue Engineering Scaffolds. *Appl. Mater. Today* **2021**, *22*, 100923.

(5) Shin, D. Y.; Kang, M. H.; Kang, I. G.; Kim, H. E.; Jeong, S. H. In vitro and in vivo evaluation of polylactic acid-based composite with tricalcium phosphate microsphere for enhanced biodegradability and osseointegration. *J. Biomater. Appl.* **2018**, *32*, 1360−1370.

(6) Planell, J. A.; Best, S. M.; Lacroix, D.; Merolli, A.*Bone Repair Biomaterials*, 1st ed.; Planell, J. A., Best, S. M., Lacroix, D., Merolli, A., Eds.; Woodhead Publishing Limited: Cambridge, 2009.

(7) Larrañaga, A.; Petisco, S.; Sarasua, J. R. Improvement of Thermal Stability and Mechanical Properties of Medical Polyester Composites by Plasma Surface Modification of the Bioactive Glass Particles. *Polym. Degrad. Stab.* **2013**, *98*, 1717−1723.

(8) Lacambra-Andreu, X.; Dergham, N.; Magallanes-Perdomo, M.; Meille, S.; Chevalier, J.; Chenal, J. M.; Maazouz, A.; Lamnawar, K. Model Composites Based on Poly(Lactic Acid) and Bioactive Glass Fillers for Bone Regeneration. *Polymers (Basel)* **2021**, *13*, 2991−17.

(9) Rich, J.; Jaakkola, T.; Tirri, T.; Närhi, T.; Yli-Urpo, A.; Seppälä, J. In vitro evaluation of poly(ε-caprolactone-co-DL-lactide)/bioactive glass composites. *Biomaterials* **2002**, *23*, 2143−2150.

(10) Blaker, J. J.; Bismarck, A.; Boccaccini, A. R.; Young, A. M.; Nazhat, S. N. Premature Degradation of Poly(α-Hydroxyesters) during Thermal Processing of Bioglass®-Containing Composites. *Acta Biomater.* **2010**, *6*, 756−762.

(11) Perrin, E.*Elaboration et Caractérisation d'un Biomatériau Bioactif et Résorbable à Base de Polulactide et de Verre Bioactif*, INSA Lyon, 2017. 2017LYSEI110.

(12) Cannio, M.; Bellucci, D.; Roether, J. A.; Boccaccini, D. N.; Cannillo, V. Bioactive Glass Applications: A Literature Review of Human Clinical Trials. *Materials (Basel)* **2021**, *14*, 5440.

(13) Sola, A.; Bellucci, D.; Cannillo, V. Functionally Graded Materials for Orthopedic Applications − an Update on Design and Manufacturing. *Biotechnol. Adv.* **2016**, *34*, 504−531.

(14) Motealleh, A.; Eqtesadi, S.; Pajares, A.; Miranda, P. Enhancing the Mechanical and in Vitro Performance of Robocast Bioglass Scaffolds by Polymeric Coatings: Effect of Polymer Composition. *J. Mech. Behav. Biomed. Mater.* **2018**, *84*, 35−45.

(15) Eqtesadi, S.; Motealleh, A.; Pajares, A.; Guiberteau, F.; Miranda, P. Improving Mechanical Properties of 13−93 Bioactive Glass Robocast Scaffold by Poly (Lactic Acid) and Poly (ε-Caprolactone) Melt Infiltration. *J. Non. Cryst. Solids* **2016**, *432*, 111−119.

(16) Loh, Q. L.; Choong, C. Three-Dimensional Scaffolds for Tissue Engineering Applications: Role of Porosity and Pore Size. *Tissue Eng. - Part B Rev.* **2013**, *19*, 485−502.

(17) Scaffaro, R.; Lopresti, F.; Maio, A.; Sutera, F.; Botta, L. Development of Polymeric Functionally Graded Scaffolds: A Brief Review. *J. Appl. Biomater. Funct. Mater.* **2017**, *15*, 107−121.

(18) Eqtesadi, S.; Motealleh, A.; Perera, F. H.; Pajares, A.; Miranda, P. Poly-(Lactic Acid) Infiltration of 45S5 Bioglass® Robocast Scaffolds: Chemical Interaction and Its Deleterious Effect in Mechanical Enhancement. *Mater. Lett.* **2016**, *163*, 196−200.

(19) Calore, A. R.; Srinivas, V.; Groenendijk, L.; Serafim, A.; Stancu, I. C.; Wilbers, A.; Leoné, N.; Sanchez, A. A.; Auhl, D.; Mota, C.; Bernaerts, K.; Harings, J. A. W.; Moroni, L. Manufacturing of Scaffolds with Interconnected Internal Open Porosity and Surface Roughness. *Acta Biomater.* **2022**, DOI: 10.1016/j.actbio.2022.07.017.

(20) Mehboob, A.; Mehboob, H.; Chang, S.-H. Evaluation of Unidirectional BGF/PLA and Mg/PLA Biodegradable Composites Bone Plates-Scaffolds Assembly for Critical Segmental Fractures Healing. *Compos. Part A Appl. Sci. Manuf.* **2020**, *135*, 105929.

(21) Mehboob, H.; Chang, S. Optimal Design of a Functionally Graded Biodegradable Composite Bone Plate by Using the Taguchi Method and Finite Element Analysis. *Compos. Struct.* **2015**, *119*, 166−173.

(22) Masoudi Rad, M.; Nouri Khorasani, S.; Ghasemi-Mobarakeh, L.; Prabhakaran, M. P.; Foroughi, M.; Kharaziha, M.; Saadatkish, N.; Ramakrishna, S. Fabrication and Characterization of Two-Layered Nano Fi Brous Membrane for Guided Bone and Tissue Regeneration Application. *Mater. Sci. Eng. C* **2017**, *80*, 75−87.

(23) Ma, R.; Fang, L.; Luo, Z.; Weng, L.; Song, S.; Zheng, R.; Sun, H.; Fu, H. Mechanical Performance and in Vivo Bioactivity of Functionally Graded PEEK−HA Biocomposite Materials. *J. Sol-Gel Sci. Technol.* **2014**, *70*, 339−345.

(24) Vergnol, G.; Ginsac, N.; Rivory, P.; Meille, S.; Chenal, J. M.; Balvay, S.; Chevalier, J.; Hartmann, D. J. In vitroandin vivoevaluation of a polylactic acid-bioactive glass composite for bone fixation devices. *J. Biomed. Mater. Res. - Part B Appl. Biomater.* **2016**, *104*, 180−191.

(25) Whyman, S.; Arif, K. M.; Potgieter, J. Design and Development of an Extrusion System for 3D Printing Biopolymer Pellets. *Int. J. Adv. Manuf. Technol.* **2018**, *96*, 3417−3428.

(26) Justino Netto, J. M.; Idogava, H. T.; Frezzatto Santos, L. E.; Silveira, Z. C.; Romio, P.; Alves, J. L. Screw-Assisted 3D Printing with Granulated Materials: A Systematic Review. *Int. J. Adv. Manuf. Technol.* **2021**, *115*, 2711−2727.

(27) Moreno Nieto, D.; Casal López, V.; Molina, S. I. Large-Format Polymeric Pellet-Based Additive Manufacturing for the Naval Industry. *Addit. Manuf.* **2018**, *23*, 79−85.

(28) Zhou, Z.; Salaoru, I.; Morris, P.; Gibbons, G. J. Additive Manufacturing of Heat-Sensitive Polymer Melt Using a Pellet-Fed Material Extrusion. *Addit. Manuf.* **2018**, *24*, 552−559.

(29) Singamneni, S.; Behera, M. P.; Truong, D.; Le Guen, M. J.; Macrae, E.; Pickering, K. Direct Extrusion 3D Printing for a Softer PLA-Based Bio-Polymer Composite in Pellet Form. *J. Mater. Res. Technol.* **2021**, *15*, 936−949.

(30) Das, A.; Gilmer, E. L.; Biria, S.; Bortner, M. J. Importance of Polymer Rheology on Material Extrusion Additive Manufacturing: Correlating Process Physics to Print Properties. *ACS Appl. Polym. Mater.* **2021**, *3*, 1218−1249.
(31) Mackay, M. E. The Importance of Rheological Behavior in the Additive Manufacturing Technique Material Extrusion. *J. Rheol. (N. Y. N. Y).* **2018**, *62*, 1549−1561.
(32) Yousfi, M.; Belhadj, A.; Lamnawar, K.; Maazouz, A.*3D Printing of PLA and PMMA Multilayered Model Polymers: An Innovative Approach for a Better-Controlled Pellet Multi-Extrusion Process*; ESAFORM2021.
(33) Lacambra-Andreu, X.; Morelle, X. P.; Maazouz, A.; Chenal, J.-M.; Lamnawar, K. Rheological investigation and modeling of healing properties during extrusion-based 3D printing of poly(lactic-acid). *Rheol. Acta* **2022**, DOI: 10.1007/s00397-022-01377-6.
(34) Dukle, A.; Murugan, D.; Nathanael, A. J.; Rangasamy, L.; Oh, T.-H. Can 3D-Printed Bioactive Glasses Be the Future of Bone Tissue Engineering? *Polymers* **2022**, *14*, 1627.
(35) Zenati, R.; Fantozzi, G.; Chevalier, J.; Arloua, M.Porous Bioactive Glass and Preparation Method Thereof; U.S. Patent. 7,709,081 BS, 2010.
(36) Michel, C.; Roux, V.; Lerouge, T.; Hauser, D.ADDITIVE-MANUFACTURING DEVICE FOR CREATING ATHREE-DI-MIENSIONAL OBJECT; AND ASSOCIATED METHOD.EP 3046750 A1, 2014.
(37) Ginsac, N.*Caractérisation de Matériaux Composite Polyacide Lactique-Bioverre Pour Application Dans La Réparation Osseuse*; INSA de Lyon, 2011.
(38) Malmgren, T.; Mays, J.; Pyda, M. Characterization of Poly(Lactic Acid) by Size Exclusion Chromatography, Differential Refractometry, Light Scattering and Thermal Analysis. *J. Therm. Anal. Calorim.* **2006**, *83*, 35−40.
(39) Astm D729Standard Test Methods for Density and Specific Gravity (Relative Density) of Plastics by Displacement. *Am. Soc. Test. Mater.***2008**, *6*. DOI: 10.1520/D0792-20.
(40) Khare, H. S.; Burris, D. L. A Quantitative Method for Measuring Nanocomposite Dispersion. *Polymer (Guildf).* **2010**, *51*, 719−729.
(41) Domander, R.; Felder, A. A.; Doube, M. BoneJ2 - Refactoring Established Research Software. *Wellcome Open Res* **2021**, *6*, 37.
(42) Harrigan, T. P.; Mann, R. W. Characterization of Microstructural Anisotropy in Orthotropic Materials Using a Second Rank Tensor. *J Mater Sci* **1984**, *19*, 761−767.
(43) Tao, Y.; Kong, F.; Li, Z.; Zhang, J.; Zhao, X.; Yin, Q.; Xing, D.; Li, P. A Review on Voids of 3D Printed Parts by Fused Filament Fabrication. *J. Mater. Res. Technol.* **2021**, *15*, 4860−4879.
(44) Codari, F.; Lazzari, S.; Soos, M.; Storti, G.; Morbidelli, M.; Moscatelli, D. Kinetics of the hydrolytic degradation of poly(lactic acid). *Polym. Degrad. Stab.* **2012**, *97*, 2460−2466.
(45) Boiko, Y. M.; Bach, A.; Lyngaae-Jørgensen, J. Self-Bonding in an Amorphous Polymer below the Glass Transition: A T-Peel Test Investigation. *J. Polym. Sci. Part B Polym. Phys.* **2004**, *42*, 1861−1867.
(46) Boiko, Y. M.; Lyngaae-Jørgensen, J. Fracture energy-fracture stress relationship for weak polymer-polymer interfaces. *Polymer (Guildf).* **2005**, *46*, 6016−6024.
(47) Spoerk, M.; Savandaiah, C.; Arbeiter, F.; Traxler, G.; Cardon, L.; Holzer, C.; Sapkota, J. Anisotropic Properties of Oriented Short Carbon Fibre Filled Polypropylene Parts Fabricated by Extrusion-Based Additive Manufacturing. *Compos. Part A Appl. Sci. Manuf.* **2018**, *113*, 95−104.